JSAE 20159719 / SAE 2015-32-0719

Development of the XMv3 High Efficiency Cycloidal Engine

D. Littera, M. Nickerson, A. Kopache, G. Machamada, C. Sun, A. Schramm, N. Medeiros, K. Becker, N. Shkolnik, A. Shkolnik
LiquidPiston, Inc.[1]

ABSTRACT

The demand for lighter, smaller, more efficient, and more powerful engines calls for a rethinking of the traditional internal combustion engine (ICE). This paper describes development progress of LiquidPiston's small rotary engine, the XMv3, which operates on a Spark-Ignited (SI) variant of its patented High Efficiency Hybrid Cycle (HEHC). This thermodynamic cycle, which combines high compression ratio (CR), constant-volume combustion, and over-expansion, has a theoretical efficiency of up to 75% using air-standard assumptions and first-law analysis. XMv3 displaces 70cc (23cc per each of three working chambers) and is gasoline fueled. The engine is simple, having only two primary moving parts, which are balanced to prevent vibration. The 'X' engine geometry utilized by XMv3 can be considered an inverted 'Wankel', retaining the traditional Wankel' rotary advantages of high power density and smooth operation, while also overcoming some of Wankel's inherent performance limitations. These include inflexible combustion chamber shape, and lubrication and emissions challenges. At this stage of development, XMv3 produces 3.2bhp at 10,000 rpm and weighs 1.7kg. Indicated mean effective pressure (IMEP) and friction mean effective pressure (FMEP) are 5.0bar and 1.0bar respectively. The maximum tested engine speed is 15,000 rpm. Preliminary durability studies show no wear problems after 1 hour of running continuously at full load. This paper details both analytical and experimental studies carried out on the XMV3 prototype, including variation of compression ratio, combustion chamber shape, spark plug type, rotor port geometry, and supercharging. With further development, the engine is expected to produce 5 horsepower at up to 15,000 RPM, weighing in at < 1.5 kg.

Figure 1: XMv3 (left) and XMv2 (right) comparison

INTRODUCTION

The internal combustion engine enjoys widespread use as an inexpensive and reliable power conversion system. Today's small piston engines can be inexpensive, and have suitable reliability to serve a variety of applications including mobile propulsive power for scooters, motorcycles, all-terrain vehicles (ATVs), boats, and small aircraft including unmanned aircraft vehicles (UAVs). Small engines are also used for power generation, including electric or auxiliary power, and to directly provide mechanical power for lawn and garden equipment. While piston engines enjoy prolific use, their efficiency is remarkably low, especially as the engine is scaled down. Literature indicates peak engine efficiencies of 12-15% for 30cc 1hp 4-stroke, and average part-load efficiency significantly lower [1].

The rotary engine has some advantages that make it a formidable contender for some markets currently served by reciprocating engines. The piston in a 4-stroke reciprocating engine momentarily comes to rest four times per cycle, as its direction of motion changes. In contrast, the moving parts in a rotary engine remain in continuous unidirectional rotational motion. High power density, smooth operation, simple design, low vibration, compact size, and reduced weight are a few of the benefits [2]. However, the rotary type engine has some drawbacks. A major problem of the Wankel rotary

[1] This research was, in part, funded by the U.S. Government. The views and conclusions contained in this document are those of the authors and should not be interpreted as representing the official policies, either expressed or implied, of the U.S. Government.

engine is that it does not measure up to the fuel economy of reciprocating engines, in part due to the long combustion chamber shape with high surface area, and low compression ratio (CR). Additionally, the gas seals of the rotary engine, such as apex and side seals, are challenging to lubricate and less efficient and durable compared to piston rings. However, seals have been steadily improved for gasoline spark-ignited (SI) rotary engines [3]-[6]. Recently, the rotary engine has become more attractive to applications where the merits of rotary engines are becoming more important, such as the continuous-growth Drones and Unmanned Aerial Vehicles (UAVs) markets, due to size, efficiency, and power density.

The LiquidPiston's 'X' architecture is a rotary engine embodiment similar in some aspects to the Wankel-type, however, several key differences lead to advantages. A primary motivation for development this engine architecture is the ability to embody an optimized 4-stroke cycle, dubbed the High Efficiency Hybrid Cycle (HEHC), which can change the operation of internal combustion engines fundamentally [7]-[9]. Figure 2 shows the components of the XMv3, where the rotor and shaft are the only primary moving parts.

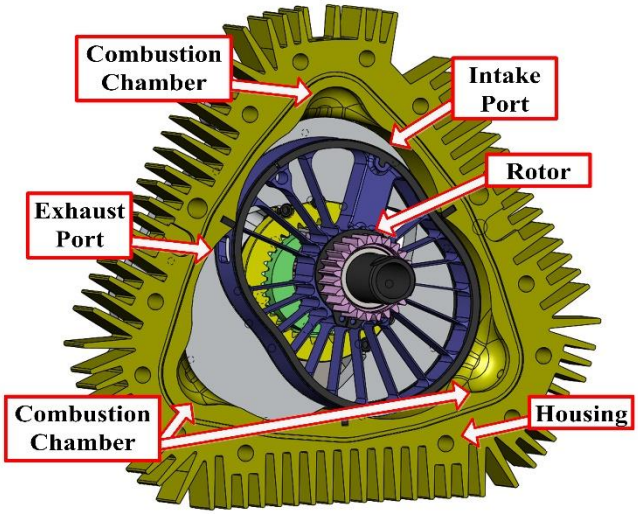

Figure 2: XMv3 Outline and components details

This paper will present the design and architecture of the XMv3 engine, which builds on prior work, and will be compared especially to the prior generation XMv2 presented in [10]. Various design considerations will be discussed. Topics presented will include durability, performance, cooling, sealing, combustion chamber design, and spark plug selection. Following the architecture section, LPI's GT-Power 1D and Converge CFD models are described. Finally, experimental methods are reviewed, and results presented for the topics introduced above. The paper is concluded with a discussion of anticipated future work.

HIGH EFFICIENCY HYRBID CYCLE (HEHC) - REVIEW

The analysis of an engine's thermodynamic cycle allows power, efficiency, and other performance parameters to be predicted. A physics-based approach to engine improvement therefore often begins with the thermodynamic cycle. From such an approach, it is apparent that typical piston SI engines only convert about 15-25% of the available fuel energy into useful mechanical work [1][11]. A first order approximation of an engine cycle can be obtained by considering "Ideal" cycle analysis using Air-standard assumptions, and the results are useful for observing trends. For example, such modeling predicts that increasing compression ratio increases engine efficiency. Additionally, constant-volume (isochoric) combustion is predicted to be more efficient than constant-pressure type of combustion. Isochoric combustion has been described as the "holy grail" of engine research by Blair [1]. A comparison by Sandia National Labs [12] shows that using ideal cycle assumptions, constant volume combustion offers a 50% improvement in power and efficiency over a constant-pressure (diesel) cycle, with all other factors equal. Finally, it is apparent from P-V diagrams that typical piston engines employing Otto and Diesel cycles still contain energy at the end of expansion, as the gas is not fully expanded. This energy is typically wasted through the exhaust process, but can also be partially recovered by turbocharging or by over-expanding, as in the Miller/Atkinson cycles.

The focus of this paper is on hardware improvements of a small SI engine which operates on the HEHC-SI cycle. An in-depth analysis of the HEHC cycle has been presented previously [7]-[10] [13]-[16]. To review, key features of the HEHC cycle include:

1) High Compression Ratio.
2) Constant Volume Combustion (obtained by introducing a dwell in the volume near the engine Top Dead Center (TDC) position).
3) Gas is over-expanded until approximately atmospheric pressure remains in the chamber.

The HEHC cycle is most effective as a compression-ignition (CI) engine operating on diesel or other heavy fuel. Under air-standard assumptions, at a CR of 18:1, the HEHC-CI cycle has ideal thermodynamic cycle efficiency of 74%, which is approximately 30% higher than comparable Otto or Diesel cycles (see Figure 3).

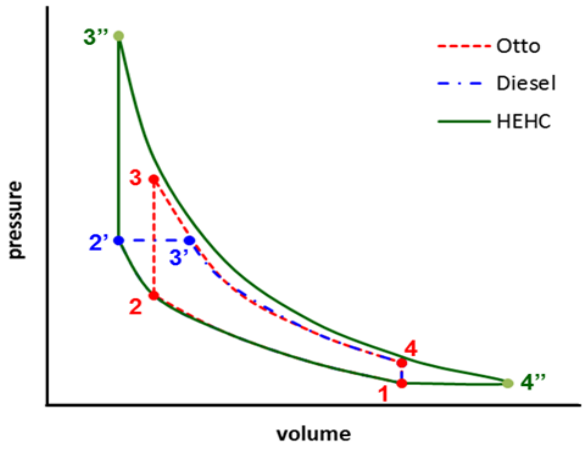

Figure 3: Thermodynamic cycle qualitatively showing HEHC vs Otto vs Diesel cycles

While LiquidPiston has CI-HEHC engines under development, in this paper, we focus on an SI version of HEHC. The compression ratio is limited to below 11:1 to avoid knock, but the other features of the cycle remain; constant-volume combustion over 20 degrees of crank shaft rotation, and over-expansion of the gasses in the chamber contribute to higher efficiencies.

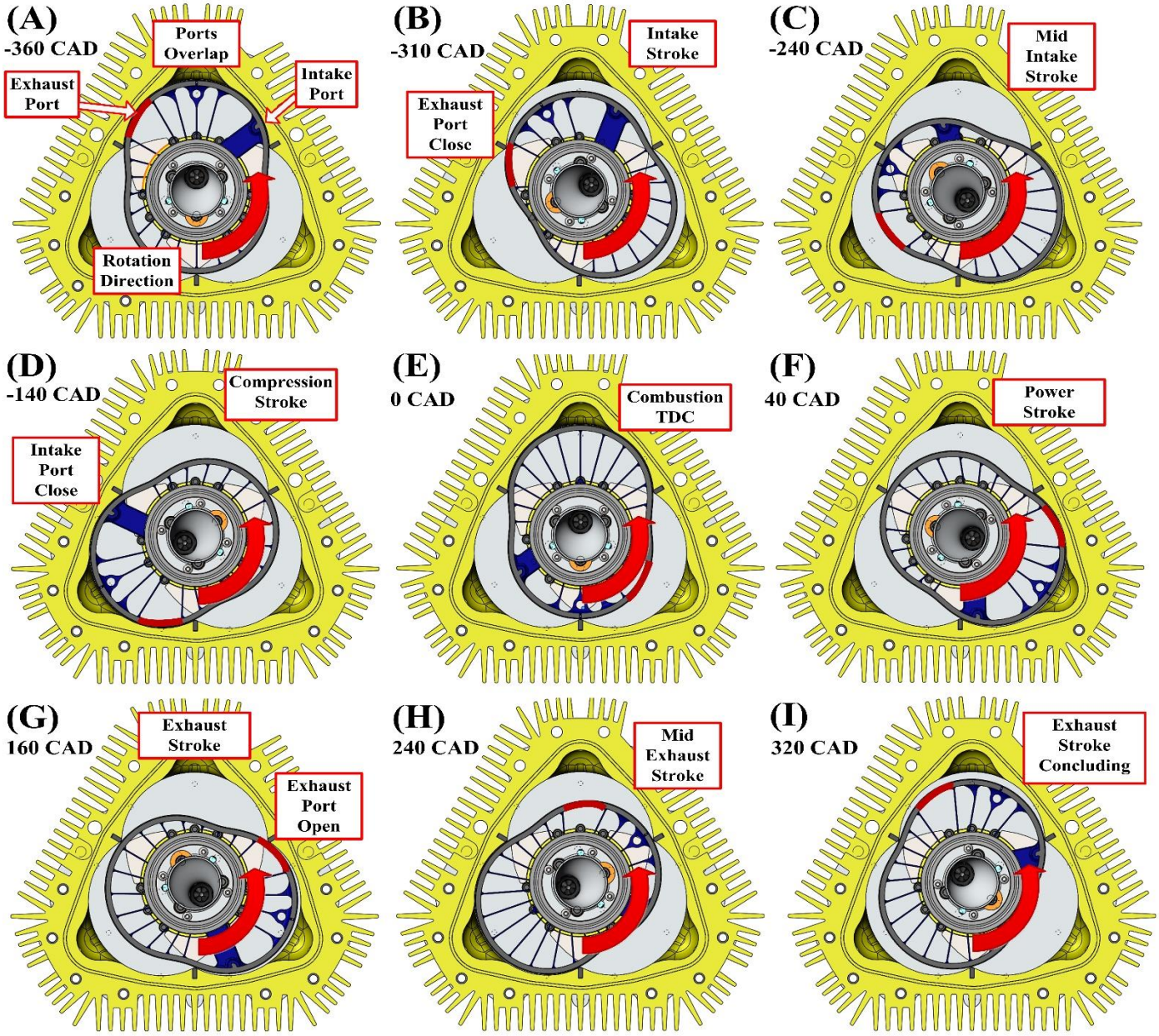

Figure 4: Operation of the XMv3 engine. In the top chamber, we follow the cycle as follows: (A) Intake begins. (B) Intake continues. (C) Note that the intake port remains open beyond the maximum volume position. The chamber volume contracts slightly before (D) Intake concludes, and Compression begins. (E) Compression finishes and combustion occurs. The arc of the rotor matches the arc of the housing, enabling constant-volume combustion. (F) Expansion / Power stroke. (G) Exhaust port opens. (H) Exhaust continues. (I) Exhaust continues, nearing completion. Intake and Exhaust overlap briefly and the cycle repeats with (A). This cycle occurs simultaneously in all three chambers.

HEHC-SI 'X' ENGINE (REVIEW)

There are many ways, theoretically, to embody a given thermodynamic cycle. LiquidPiston has explored numerous such embodiments (engine architectures) to embody the HEHC cycle, and has converged on a simple rotary engine dubbed the 'X' engine.

For a thorough description of the X engine, the interested reader is referred to SAE Paper [10], and to an animation of the (CI) version of the engine operation: http://liquidpiston.com/technology/how-it-works/. The HEHC Model X engine employs a four-stroke cycle incorporating intake, compression, expansion, and exhaust. Each of these strokes occurs sequentially within each of the three engine chambers (see Figure 4). The engine is ported in a unique way, with gas exchange routed through channels in the rotor. This allows 4-stroke operation without the use of poppet valves. During the intake stroke, air and fuel are first routed through the crankshaft, and then radially out through a channel in the rotor, with a port in the rotor accessing a given working chamber. After the expansion stroke, exhaust products are routed radially in through an exhaust port within the rotor and then axially through a side cover to the exhaust collector. Asymmetry in the locations of intake and exhaust ports (relative to the rotor centerline) enables over-expansion. As in a piston engine using valve timing to achieve Miller or Atkinson cycles, the X engine working chamber volume at Intake Port Closing (IPC) is significantly smaller than at Exhaust Port Opening (EPO). Constant-volume combustion is achieved (without complex mechanisms) by trapping air/fuel mixture within each of the combustion chambers for a prolonged period while the rotor is spinning near TDC. This is enabled by the 'X' engine geometry, wherein the arc of the

rotor profile matches closely to the arc of the housing profile, and so the rotor can turn near TDC with all gasses remaining in an isolated (stationary) combustion chamber within the housing while volume remains approximately constant. Thus, the unique aspects of the engine geometry allow the engine to embody the HEHC.

XMv3 was designed primarily for low-vibration, lower noise, and high power density applications. XMv3 presents minimal "freeze" over a regular piston engines to achieve HEHC due to the high combustion speed of gasoline. On the other hand, when operating with diesel, different epicycloid design parameters allow engine geometries with longer dwell times. The port timing of the XMv3 engine utilizes an effective expansion vs compression ratio of 1.15. With different port locations, larger over-expansion ratios are possible which would be closer to the ideal cycle. The XMv3 port timings are selected to maximize power density rather than fuel efficiency.

HARDWARE IMPROVEMENTS

XMV3 ARCHITECTURE

For comparison, the cross section of XMv2 (previously presented in [10]) is shown in Figure 6. After initial testing, it became clear that the performance of XMv2 could be improved by several major design changes. The durability, performance, and cooling of the engine are improved in the new XMv3 architecture, shown in Figure 7, while maintaining the advantages of small size, low vibration, high power density, etc. XMv3 performance is compared to XMv2 in Table 1, and both engines are shown side by side in Figure 5 and Figure 1.

Durability: The XMv2 utilized a 3-piece shaft, with each piece being supported by two bearings, allowing relative motion in the assembly. For XMv3, the 3-piece shaft is replaced by a 2-piece shaft, and the pieces are rigidly fastened to prevent relative motion, thus increasing the mechanical stiffness of the engine (see Figure 7). The new crankshaft reduces dynamic rotor displacement caused by gas pressure, allowing for tighter clearances and therefore better gas sealing. The fatigue life of the rotating components is also increased. Due to a better distribution of load, XMv2's bearing journal wear has been eliminated. Another major durability improvement is related to bearing selection. Using empirical data from XMv2 testing, accurate bearing loads and fatigue lives for XMv3's components were calculated, and the total number of bearings reduced from five to four. Finally, cooling fins are added to the aluminum engine housing, and the rotor material is changed from aluminum to steel. The mechanical properties of steel allow the rotor to better withstand seal contact and the combustion environment, while maintaining the same weight as XMv2's aluminum rotor.

Figure 5: XMv2 (left) and XMv3 (right) comparison

Performance: As the engine breathes through the crankshaft, the more robust design also increases the minimum intake flow area, allowing more air into the engine. Restrictions in the intake system are further reduced by smoothing the intake pathway and removing sharp transitions. The friction of the engine is lowered by changing the type and number of bearings and oil seals. There are several developments in sealing and combustion chamber shape which contribute to higher engine performance. The weight has been reduced by 6%, from 1.8kg (XMv2) to 1.7kg (XMv3), while targeting 1.5kg for the production ready version. The engine housing and side covers remain overbuilt for prototype purposes but can later be optimized for size and weight.

Table 1: XMv2, XMv3 Performance and Specifications Summary

Configuration	XMv2	XMv3
Engine Displacement	69cc	
Fuel Type	50:1 Gasoline:Oil Mixture	
CR	11:1	
Trapped CR*	9.52:1	
ER	11:1	
Max Brake Power	1.00hp@ 8000rpm	3.23hp @ 10000rpm
BMEP	1.6 bar	4.0 bar
FMEP	1.0 bar	1.0 bar
IMEP	2.6 bar	5.0 bar
Max Engine Speed	10000rpm	15000rpm
Weight	1.81kg	1.71kg
Ignition	3 spark plugs with ECU	
Fueling	Port Fuel Injection	
Cooling	Internal and External air	
Durability	5m full load	1hr full load

** Trapped CR is referenced to trapped volume at Intake Port Close (IPC)*

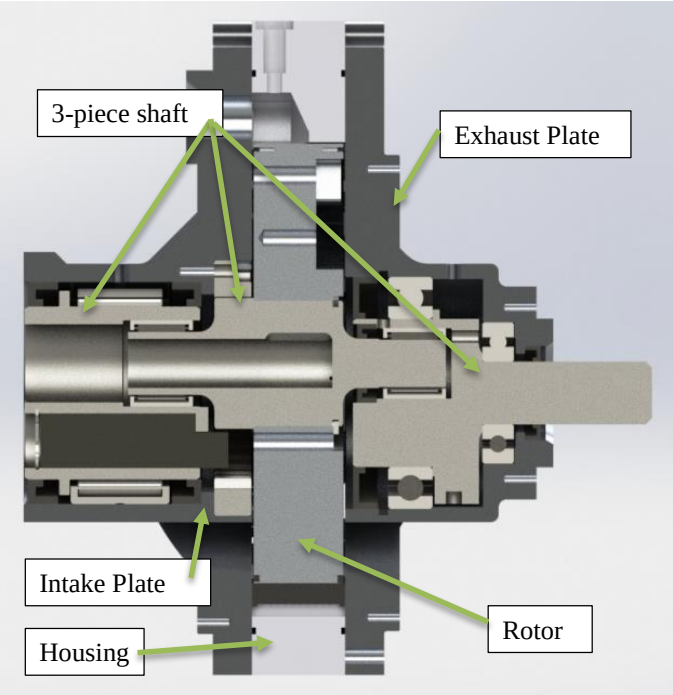

Figure 6: XMv2 cross section (spark plugs not shown)

Cooling: Advances in cooling allow XMv3 to run steady state at 10,000 RPM, WOT with air cooling. This is achieved through the use of cooling shrouds which direct air to the housing and rotor in proper proportions. Rotor cooling is improved by increasing surface area and by altering the air pathway and residence time to maximize heat transfer. Fins are added to the housing, increasing surface area. Some of the methods tested are adapted from the heat exchanger industry, while others have been developed in-house. Through these developments, the cooling airflow rate and fan power requirements are approaching numbers typical for those of small air-cooled piston engines

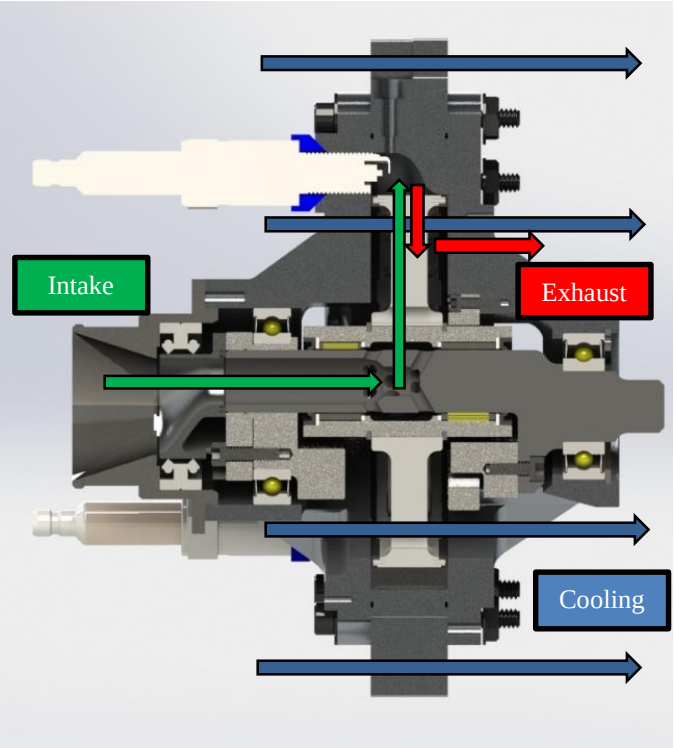

Figure 7: XMv3 cross section with flow path

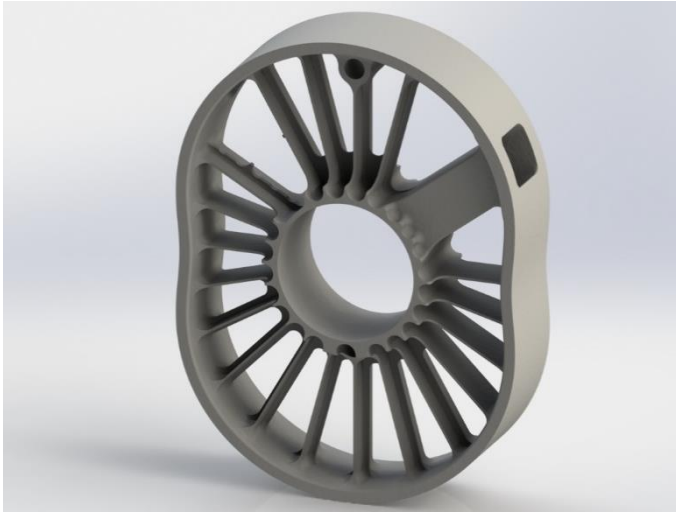

Figure 8: XMv3 steel rotor with internal support / cooling ribs. Seals not shown.

Sealing: A well-known challenge in any rotary engine is the gas sealing of the working chambers. XMv2 architecture followed the traditional Wankel approach for both face and apex seals, referred to here as *"internal"* face seals. The fundamental difference in geometry between the 'X' configuration and Wankel called for a modified solution. The "U-cup" face seal (see Figure 9), and then "U-cup second generation" seals provide a nearly perfect geometric sealing grid, resulting in improved engine performance. While piston engines can be nearly perfectly sealed (geometrically, e.g. neglecting manufacturing and thermal distortions), the same was not true for Wankel rotary engines which had known leak paths between the face seals and button /corner seals.

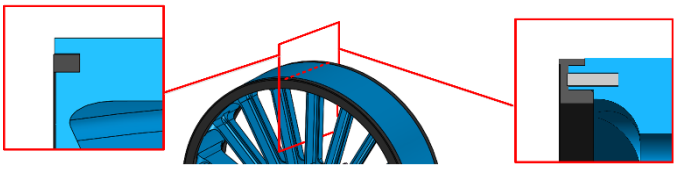

Figure 9: Cross section of the XMv3 U-cup face seal (right) and previous XMv2 internal face seal (left)

Combustion Chamber: the lack of poppet valves in rotary engines is desirable because it increases simplicity and durability, but these advantages come at the expense of intake flow control in the engine. Without an intake valve, it becomes more difficult to manipulate swirl and tumble, which affect mixing, turbulence, and ultimately combustion performance.

The bulk of piston engines generate swirl and tumble motion during the intake stroke, which persists until ignition as a result of flow momentum [16] [17] [19] [20] [21] [22]. The turbulence kinetic energy (TKE) associated with the flow is at its peak during the intake stroke and tends to reduce by the time ignition takes place. A unique capability of the XMv3 architecture is to fully displace the air and fuel mixture into a chamber of any size or geometry, favoring squish as a more effective way to generate swirl and tumble just prior to ignition, when compared to a piston engine:

$$\frac{TKE}{m} = \frac{1}{2}\left(\overline{u'^2} + \overline{v'^2} + \overline{w'^2}\right)$$ *Equation 1*

Two different type of chambers are evaluated in this paper, the first one called *"quiescent"* has a symmetrical recessed dome shape which provides a quiescent velocity field (see Figure 10) while the second one called *"high-speed"* is asymmetrical to generate a strong swirl motion at TDC (see Figure 11). Some CFD and combustion results applying these two chamber designs are presented in corresponding sections below.

Figure 10: XMv3 quiescent combustion chamber

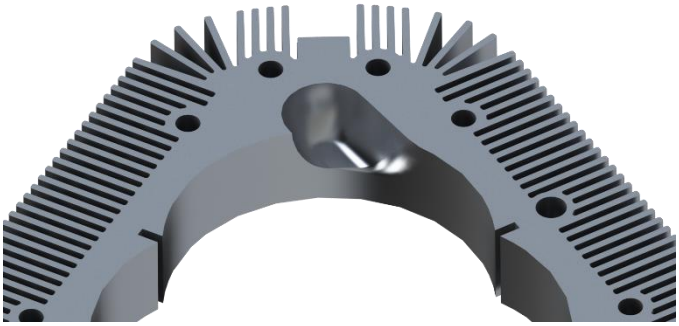

Figure 11: XMv3 high speed combustion chamber

Pulstar® Spark Plugs:

Pulstar® Pulse Plugs have a capacitor in the core that stores energy from the ignition coil. Immediately before the spark, Pulstar® with PlasmaCore Plugs release this energy in a quicker and more powerful burst than regular spark plugs. The plasma field sensitizes the fuel mixture allowing it to burn more quickly and completely once the spark is formed, creating consistent cycle-to-cycle combustion pressure resulting in a better combustion. These results are verified in XMv3 test data, with results presented below.

MODELING

Computational fluid-dynamics (CFD) and 1-dimensional engine modeling software are used for the analyses of test data and also as predictive tools.

GT-POWER MODEL

A 1-dimensional model of the X-mini rotary engine has been developed using Gamma Technology's GT-Power. Using piston and cylinder approximations of each chamber, and custom functions, an approximation of the rotary XMv3 is achieved. A top-level overview of the model is seen in Figure 12. The model begins with inlet at the intake plenum (green box) and exhausts to the engine shrouds (red box). Intake and exhaust tracts are modeled as closely as possible to the experimental setup. This process involves 1-dimensionally discretizing some of the complex parts, such as the cooling and exhaust paths through the rotor (using GEM3D). The working chambers are modelled as crank-less pistons and cylinders. A piston position array was used to overcome the variations of the rotary volume profile versus a crank-slider profile. A customized process was developed to modify GT-Power's internal heat transfer correlations for the 'X' engine, and a surface area correction factor was generated.

Test data was used to calibrate and validate the model. Parameters used in calibration include a heat transfer constant, equivalent critical orifice for "atmospheric" leak area (modeling blow-by across the face seal), and "inter-chamber" leak area (modeling leakage from one chamber to the adjacent chamber presumably across the corners of the apex seals). These parameters can be calibrated to match experimental motoring traces, and then lumped in with heat release parameters while fitting firing traces. Heat release can be calculated using single or multiple Wiebe functions, individual instantaneous heat release rate parameters, or custom heat release profiles. The results section shows a typical calibration validation curve where mass airflow values across a range of speeds during motoring are compared to experimental values. This model offers insight into the engine's operation, identifying clearly where energy and mass flow within the system. Once calibrated, the GT Power model is a useful predictive and optimization tool.

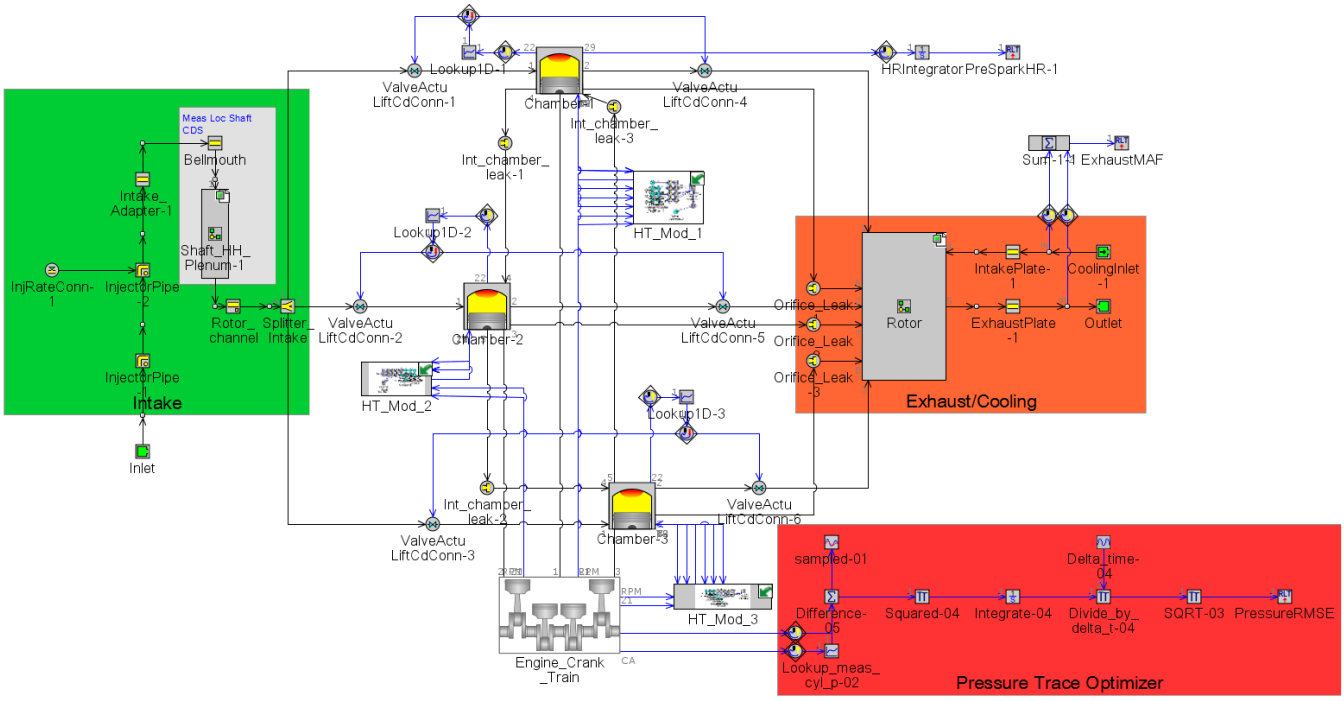

Figure 12 :XMv3 GT-Power model schematic

CONVERGE CFD

The CFD software CONVERGE developed by Convergent Science was used to study the complex flow with the XMv3 engine. This powerful tool allows for meshing of moving boundaries and disconnecting sections.

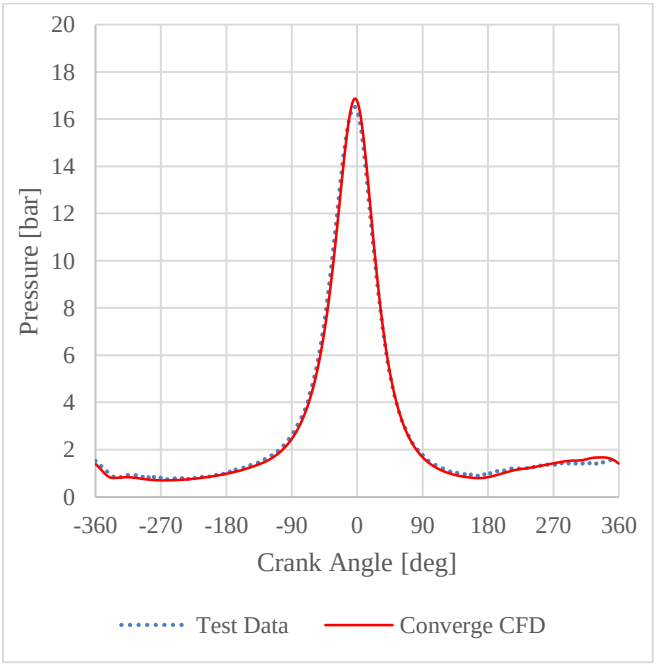

Figure 13: Motoring Pressure trace matching for Converge CFD Model and Test Data at 10,000rpm

A finite volume, second-order accurate spatial scheme was used to solve all transport and momentum equations. Time step determination was handled dynamically by the code with a set range between 1.0e-05 to 1.0e-07 seconds. The time step was calculated for each cycle based on Courant-Friedrichs-Lewy (CFL) numbers. For both the convective and diffusive CFL numbers, 2 was used during the simulations. For the speed of sound, CFL = 50 was used.

The simulated fluid was a homogenous stoichiometric mixture of air and iso-octane. Temperature and pressure boundary conditions were applied to the inlet of the intake pipe and the exit of the exhaust windows. These properties were taken from test-cell conditions obtained at the same locations on the experimental setup. The Renormalization Group k-e (RNG k-e) turbulence model was included.

The results were taken from the last cycle of a sequence of three cycles; the first used a coarse mesh (2.6 mm) and the two following used fine mesh (1 mm), arranged in a uniform, orthogonal, cut-cell Cartesian grid. Permanent mesh refinement was specified along the engine chamber and rotor walls to maintain the y^+ values in the appropriate range, between 30 and 100.

In order to simulate the face and apex seals of the engine, CONVERGE's sealing capability was used. This function was instrumental to the model, due to the rotating and translating behavior of the face seals. Three different seals were used to define the three separate working chambers. One seal was located on each of the three apex boundaries, directed towards the rotor surface. The other two were placed along each side of the combustion chamber/housing profile directed towards the intake and exhaust side plates. A value of 5.0e-05 m was use as sealing tolerance.

EXPERIMENTAL METHODOLOGY

Engine experiments were conducted at LiquidPiston's engine dynamometer test facility. Figure 14 shows an instrumented XMv3 engine on the dynamometer. Plastic shrouds are used to direct the cooling air to and from the engine. The test cell

and laboratory is operated and maintained according to the indications and recommendations of the code of federal regulation (CFR 40 part 1065). The engine is operated using a custom DRIVVEN control system capable of actuating start-of-injection (SOI) timing, injection duration, fuel pressure, and number of injection events. The DRIVVEN system also allows recording both high speed data (crank angle–resolved signals such as chamber pressures, injector current signals, instantaneous engine torque, etc.) and low speed data (time-based signals such as intake air temperature, exhaust gas temperature, oil pressure, etc.). In-chamber pressure measurements are performed in each chamber using Kistler 6052C piezoelectric pressure transducers. Typically fifty engine cycles are acquired and averaged for each steady-state condition. Commercially available premix fuel 50:1 with minimum octane rating of 92 (R+M)/2 was used during the entire test campaign. The fuel uses synthetic oil for lubrication and it is ethanol free. The test cell is also equipped with California Analytical Instruments (CAI) emission bench capable to analyze CO_2, CO, HC and O_2 from the raw exhaust. This bench will be used for the finer tuning required for the engine emission compliancy calibration.

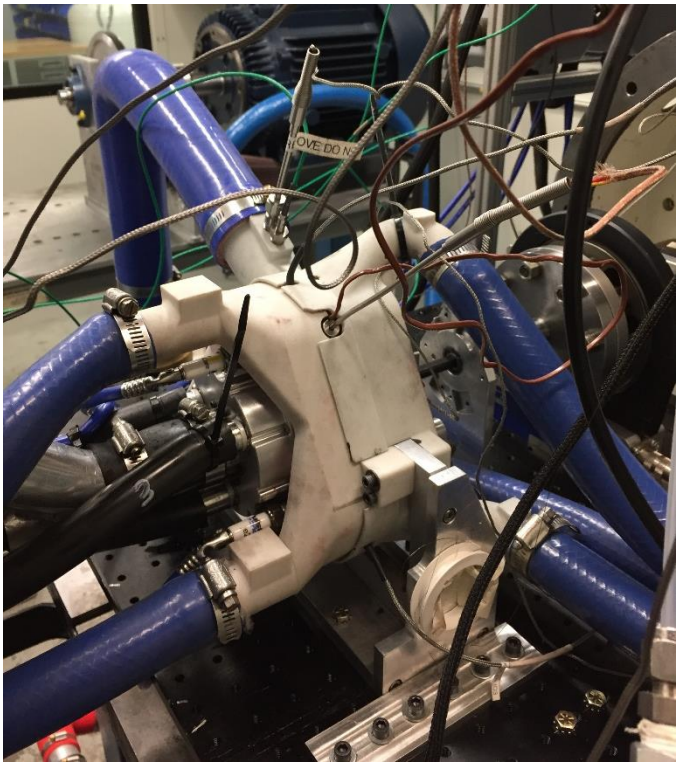

Figure 14: XMv3 installed on the dynamometer

RESULTS

FACE SEALS

Figure 15 shows sealing improvement from XMv2 (internal face seals), to XMv3 with internal face seals, and a further improvement to XMv3 with U-cup (external) face seals. On the same plot, a commercially available 30cc 4-stroke piston engine peak motoring trace is shown (note the trapped CR of the 4-stroke engine was 8.4, while for XMv3 it was 9.5). Gas sealing improvements translate to improvements in engine power; XMv2 produced 1bhp at 8000rpm, while XMv3 produces 3.2hp at 10000rpm.

The second generation U-cup seal was tested at a lower trapped CR of 8. Figure 16 shows a comparison of peak motoring pressures for the two generations of U-cup face seals, marking an additional 12% improvement up to 9000rpm. Figure 17 shows the improvements of the second generation seals on the trapped volumetric efficiency, quantifiable up to 34% at 9,000rpm, allowed by a reduction in inter-chamber leak. Firing tests with the second generation U-cup seal have not yet been performed, and the development of still better performing seals is ongoing.

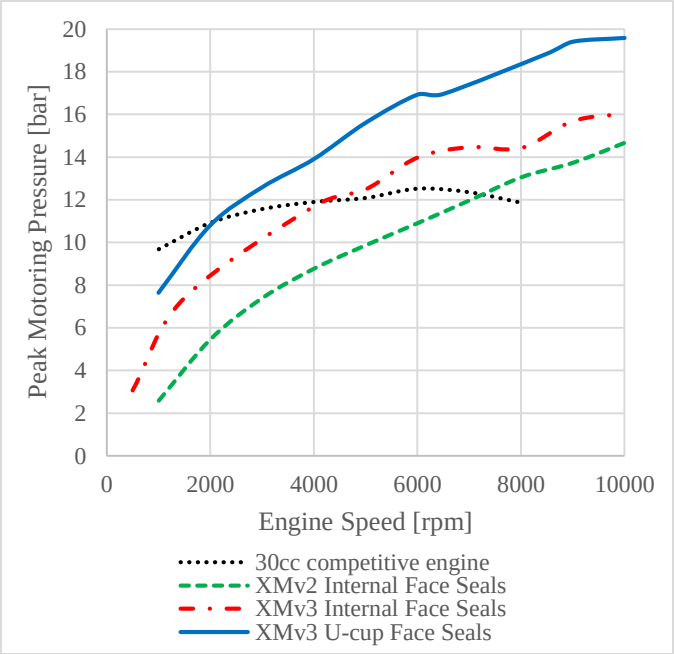

Figure 15: Peak motoring pressures for XMv2, XMv3, and 30cc competitive piston engine, trapped CR is equivalent to 9.5

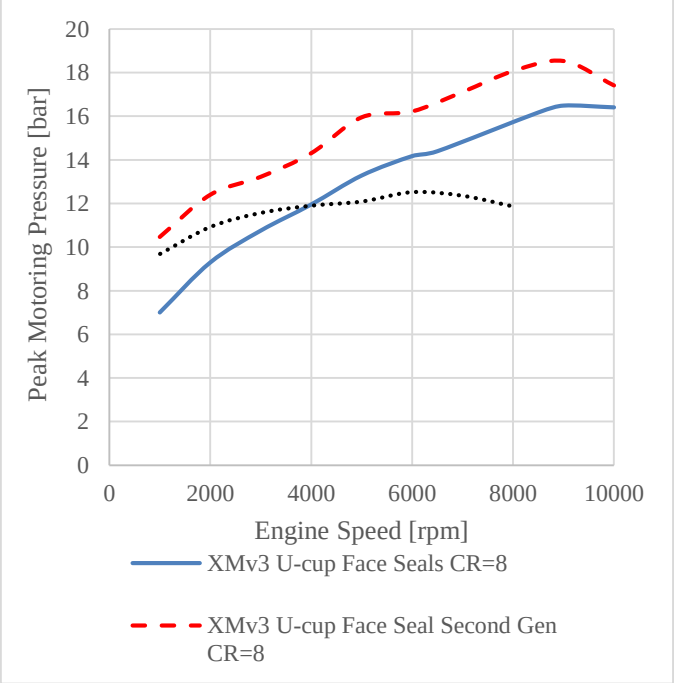

Figure 16: Peak motoring pressures for XMv3 U-cup face seal first and second generations. The trapped CR is 8.0 in both cases.

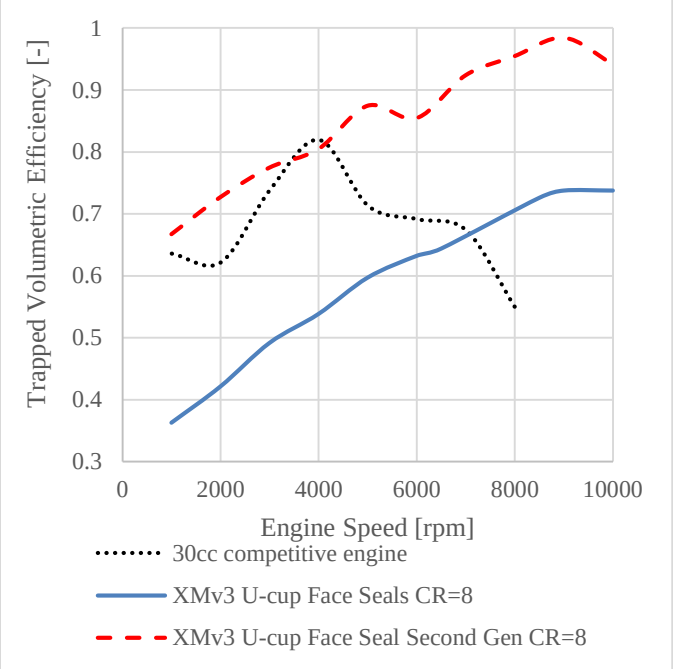

Figure 17: Intake mass airflow comparison between the two generations of U-cup face seals

HIGH SPEED COMBUSTION CHAMBER

The CFD results indicate an increase in charge speed (at TDC) by one order of magnitude between the "quiescent" and "high-speed" chambers, from 4 to 40 m/s respectively (see Figure 18 and Figure 19). The value of 40 m/s achieved with the high-speed chamber is greater than the average (30m/s) generally observed in direct injection (DI) engines with squish ratios of 0.7 [16]. The spark plug in the high-speed chamber is placed in the eye of the cyclone, reducing the chance of misfire followed by a quick spreading of the combustion throughout the chamber. Figure 20 and Figure 21 show how the TKE is distributed in the two chambers. The high-speed chamber provides higher values with a doughnut shape (following the vortex flow), while the quiescent chamber results in a spherical shape with lower values.

Figure 22 shows that TKE has a similar trend during intake stroke (0-180 deg). During compression, the high-speed chamber already has a slightly higher TKE, but only during the squish the (330-360 deg) does the TKE drastically increase (see the zoomed window in Figure 22). TKE in the quiescent chamber is 9.1 m^2/s^2 just prior the ignition, while the high-speed chamber presents a peak of 15.25 m^2/s^2, an improvement of 68%. More interestingly, at TDC, this improvement is much greater. The TKE in the quiescent chamber is 6.66 m^2/s^2, while the high-speed chamber achieves a peak of 12.52 m^2/s^2, an improvement of 88%.

The effects of TKE on combustion are radical (see Figure 23 and

Figure 24); the peak combustion pressure increases from 40 to 49 bar, indicating a faster combustion. Figure 25 shows how the high-speed chamber has a faster heat release rate, and consequently shorter combustion duration. The combustion duration (10% to 90% MFB) is reduced from 22 to 15 CAD at 10,000rpm. Unfortunately, this faster combustion, with higher peak pressures and temperatures, causes increased heat and mass leakage, resulting in lower brake power, 2.4 vs. 3.2hp. On the other hand, the higher TKE reduced the coefficient of variation (COV) of IMEP from 5.2% to 3.5%. It is important to remark that the quiescent chamber presented an effective CR of 9.5 while the high-speed chamber was 8.6. Improved sealing will help to fulfill the potential of the high-speed chamber, allowing higher power output and fuel efficiency. These two chambers represent extremes in TKE; a chamber having additional features, which optimizes combustion processes is currently being designed.

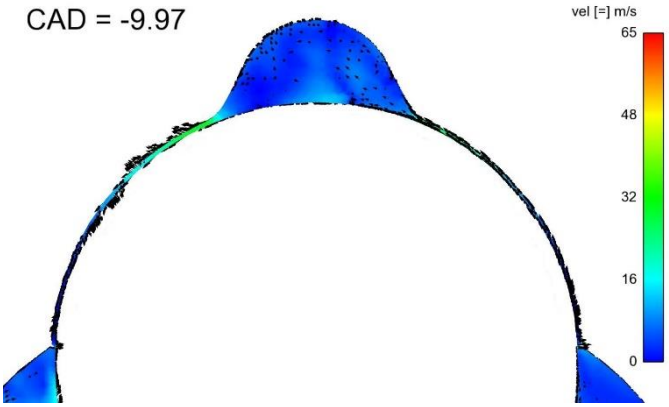

Figure 18: Velocity magnitude contour plot for the quiescent chamber at 10deg BTDC, indicating a quiescent chamber just before spark at 10,000rpm

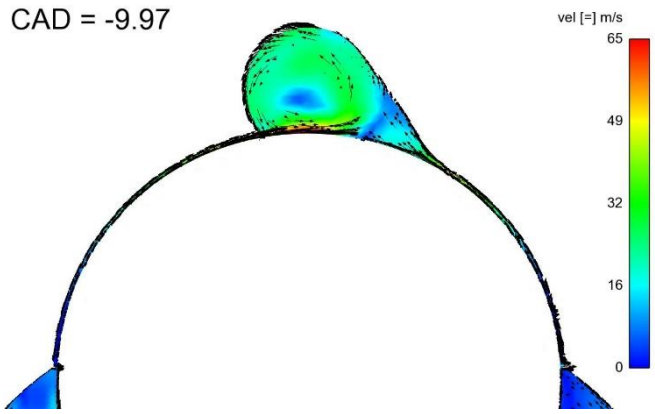

Figure 19: Velocity magnitude contour plot for the high velocity chamber at 10deg BTDC, indicating a strong swirl in the chamber just before spark at 10,000rpm

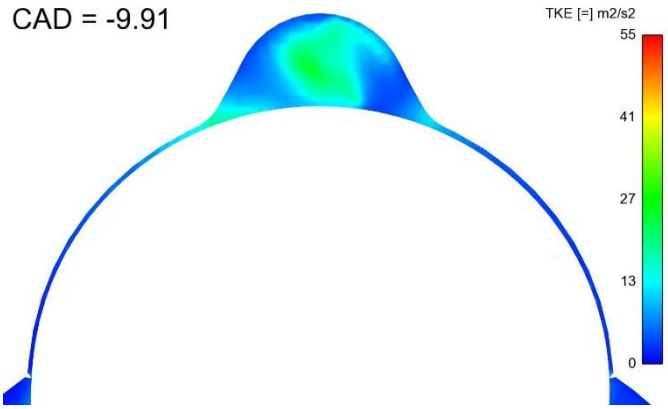

Figure 20: Magnitude TKE contour plot for the quiescent chamber at 10deg BTDC, indicating a quiescent chamber just before spark at 10,000rpm

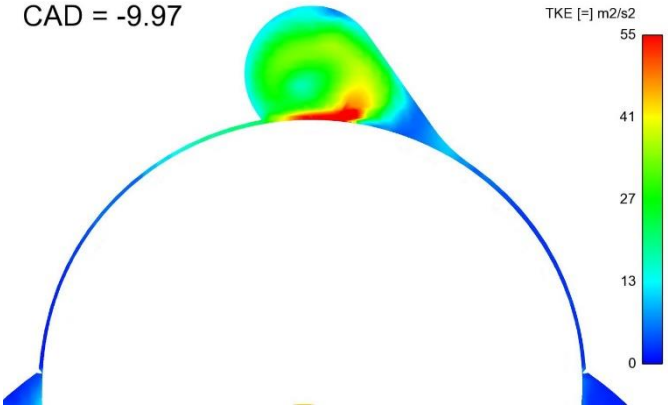

Figure 21: TKE magnitude contour plot for the high velocity chamber at 10deg BTDC, indicating a strong swirl in the chamber just before spark at 10,000rpm

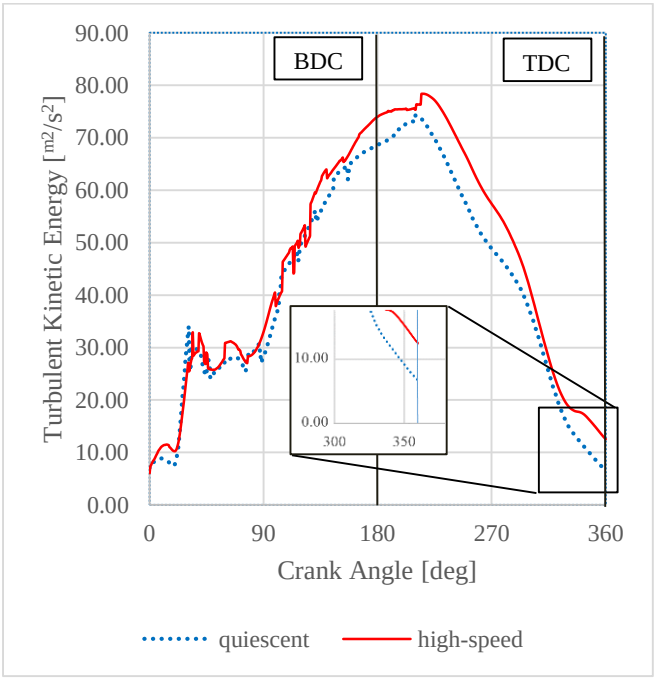

Figure 22: TKE plot versus crank angle of the two chambers at 10,000rpm

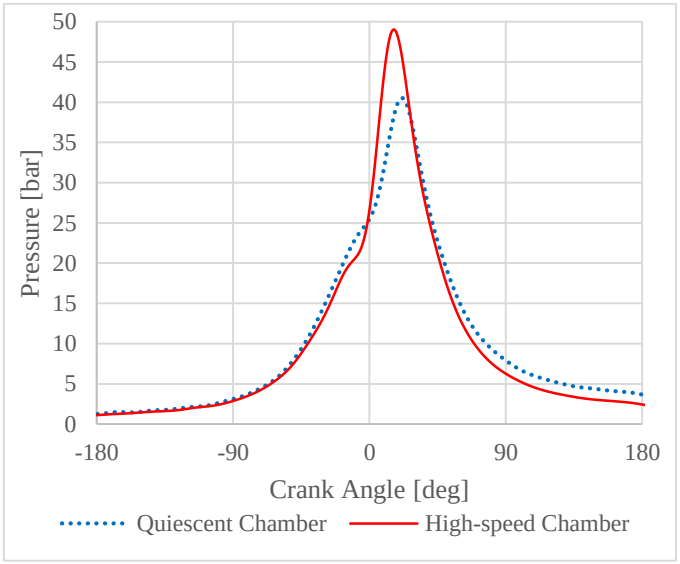

Figure 23: Comparison of the combustion pressure trace for the quiescent and the high-speed chamber at 10,000rpm

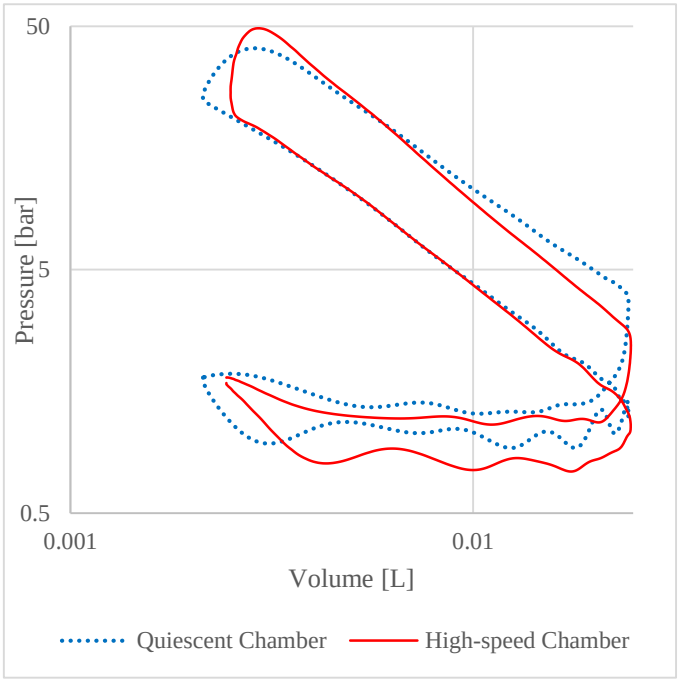

Figure 24: Comparison of the logarithmic P-V diagram of the combustion trace of the quiescent and high-speed chamber at 10,000rpm

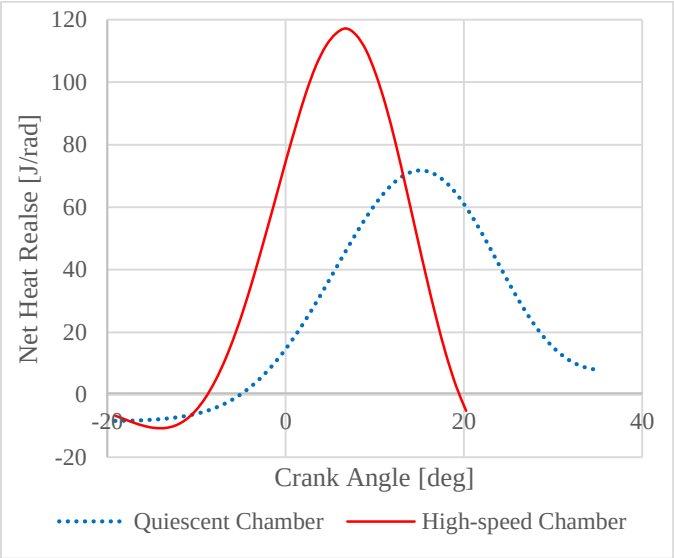

Figure 25: Comparison of the net heat release rate for the quiescent and the high-speed chamber at 10,000rpm

PULSTAR® SPARK PLUGS

The different shape of the common spark plugs and the Pulstar® caused a minimal difference in compression ratio. Test results indicate an increase of indicated power from 3.25hp to 3.59hp, or an improvement of 10.5%, while the COV of IMEP was reduced from 6.4% to 5.3% (see Figure 26 and Figure 27). The heat release rate for the Pulstar® Spark plugs shows faster combustion, with a 10% to 90% burn duration that decrease from 26.5CAD to 22CAD, equal to a 17% reduction.

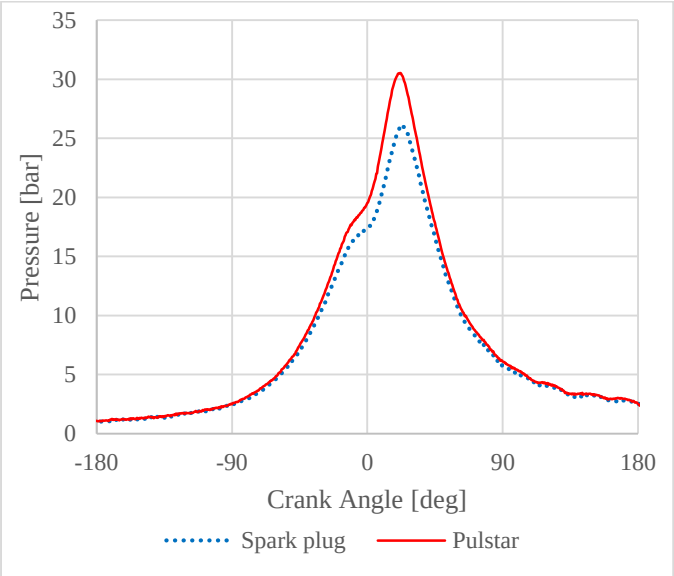

Figure 26: Comparison of the combustion pressure trace for the common and the Pulstar® spark plugs at 10,000rpm

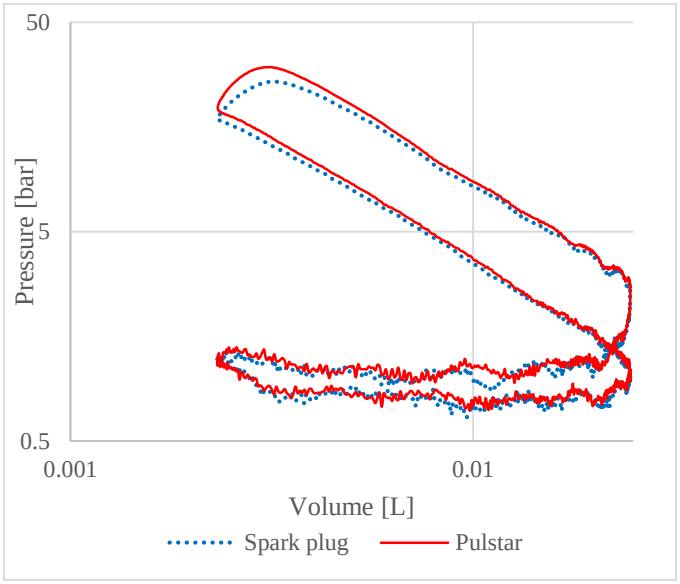

Figure 27: Comparison of the logarithmic P-V diagram of the combustion trace of the common and the Pulstar® spark plugs at 10,000rpm

DURABILITY

The durability of the engine was directly affected by the improved cooling strategy, allowing the new hardware to withstand 1hr of WOT at 10,000rpm, while producing constantly 3.2 horsepower. Upon disassembly, minimal wear is observed. This achievement is considered a positive result by the company for this stage of development. One side of the rotor is facing gas exchange phase while the other goes thru compression ignition and expansion. In spite of this heterogeneity in thermal loads, minimal differences in wear on the two sides of the rotor are observed when proper cooling is adopted. The differential thermal expansion is accounted during the design phase. The lack of poppet valve or any hot spots in the combustion chamber in conjunction with high engine speed (up to 15,000rpm) greatly reduces the chance of engine knocking, which has not been measured in CR up to 11.

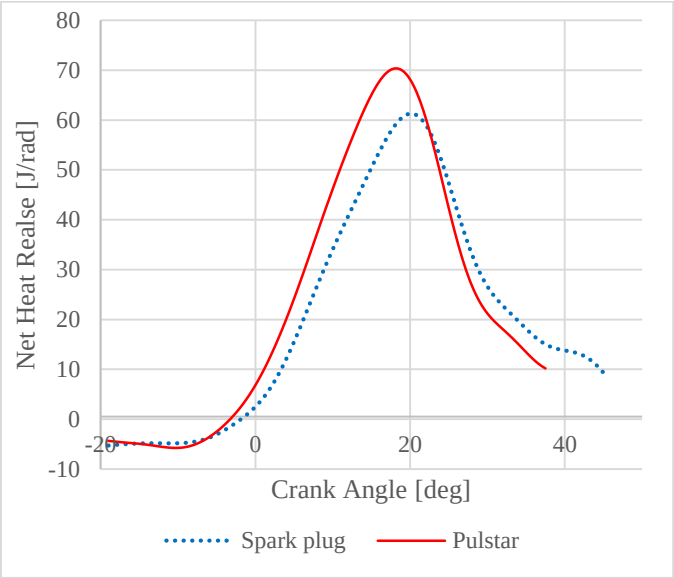

Figure 28: Comparison of the net heat release rate for the common and the Pulstar® spark plugs at 10,000rpm

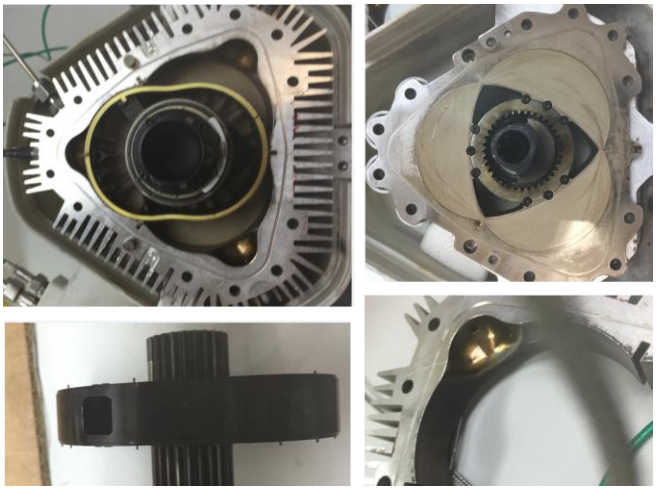

Figure 29: XMv3 Hardware following 60 minutes of steady state W.O.T. firing. All parts are in good condition with minimal wear. Top Left: Rotor with seal in housing. Top Right: Intake Side Cover. Bottom Left: Rotor. Bottom right: quiescent chamber.

FUTURE WORK

LPI's target is to achieve higher efficiency through further improvements in combustion, reduction of cooling losses, and better sealing. The indicated efficiency of a conventional small engine is compared to the SI-HEHC (CR 9.5) engine in Figure . Ideal cycle efficiency increases from 58% to 66%. While conventional small piston engines do not exceed 30% indicated efficiency, the current "X-Mini" engine 70cc gasoline SI prototype is measuring 22% net indicated efficiency in the lab, and is expected to reach 34% by extending over-expansion, improving sealing, and reducing thermal losses. Future investigations involves the analysis of Exhaust Gas Recirculation (EGR) and gaseous emissions, as means to improve combustion and efficiency. Preliminary results (not presented here) show potential for XMv3 operating on Compressions Ignition Diesel HEHC.

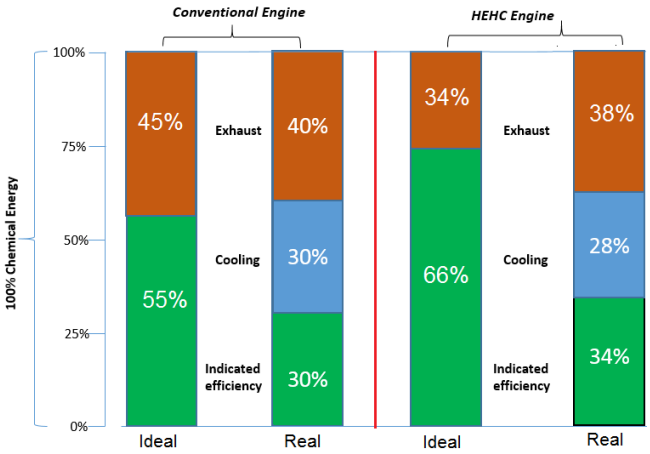

Figure 29: XMv3 engine efficiency pathway

SUMMARY/CONCLUSIONS

This paper describes recent developments of LiquidPiston's XMv3 engine, including improvements to gas sealing, combustion, and durability. These improvements bring the X architecture one step closer to fulfilling the potential of LiquidPiston's HEHC cycle.

Sealing improvements provide the greatest performance increases, and are accomplished by replacing the traditional Wankel-style face seals with LPI's patent-pending U-cup designs. The improved sealing directly affects the power output, with brake power increasing from 1.00hp @8000rpm to 3.2hp @10,000rpm for first generation hardware. The durability established at WOT increases from 5 minutes to >1 hour as a result of the U-cup seals and the rotor material change from aluminum to steel. The second generation U-cup seal, with additional peak motoring pressure increase of 12% and trapped VE increase of 34%, shows a potential path to further increase power and efficiency.

The unique capability of the X architecture to fully displace the working charge into a chamber of any shape allowed the team to test a high speed and TKE combustion chamber. Experimental results show a reduction in combustion duration from 22 to 15 CAD when compared to the quiescent chamber. Meanwhile, the high-speed chamber reduces the COV IMEP from 5.2% to 3.5%. Unfortunately, engine power output is not improved from this change, as further optimization is required.

Positive results are achieved with the use of Pulstar Spark plugs, which shorten burn duration from 26.5 CAD to 22 CAD and lower COV IMEP from 6.4% to 5.3%, and increase indicated power from 3.3hp to 3.6hp.

LiquidPiston's future work on the XMv3 targets 34% indicated efficiency by extending over-expansion, improving sealing, and reducing thermal losses. Additional work is required to verify quiet operation of the engine, mapping the engine at partial loads, and to meet emissions standards.

REFERENCES

[1] Blair, G., “Design and Simulation of Four-Stroke Engines”, Society of Automotive Engineers, Warrendale, PA, 1999.

[2] Norbye, Jan P. “The Wankel Engine”, Bailey & Swinfen, 1971, http://dx.doi.org/10.4271/R-186.

[3] Yamamoto, K., Rotary Engine, Toyo Kogyo Co., Japan, 1971.

[4] Ohkubo, M., Tashima, S., Shimizu, R., Fuse, S., and Ebino, H., “Developed Technologies of the New Rotary Engine (RENESIS)”, SAE Technical Paper 2004-01-1790, 2004, doi:10.4271/2004-01-1790.

[5] Muroki, T. and Miyata, J., “Material Technology Development Applied to Rotary Engine at Mazda”, SAE Technical Paper 860560, 1986, doi:10.4271/860560.

[6] Froede, W., "The NSU-Wankel Rotating Combustion Engine," SAE Technical Paper 610017, 1961, doi:10.4271/610017.

[7] Shkolnik, N., “Internal Combustion Power System”, US Patent 7,191,738, 2003.

[8] Shkolnik, A. and Shkolnik, N., “High Efficiency Hybrid Cycle (HEHC) Thermodynamic Cycle”, US Patent 8,365,698 , 2007.

[9] Shkolnik, A. and Shkolnik, N., “High Efficiency Hybrid Cycle (HEHC) X Engine”, PCT Patent Application: US2012-0294747 , 2012.

[10] Shkolnik, A., Littera, D., Nickerson, M., Shkolnik, N. et al., "Development of a Small Rotary SI/CI Combustion Engine," SAE Technical Paper 2014-32-0104, 2014, doi:10.4271/2014-32-0104.

[11] Heywood, J., “Internal Combustion Engine Fundamentals”, McGraw-Hill, New York, 1988.

[12] Van Blarigan ,P., Goldsborough, S., “Toward the Development of a Thermodynamic Fuel Cell, Sandia National Laboratories. Hydrogen, Fuel Cells & Infrastructure Technologies Program, Merit Review and Peer Evaluation, May 19 19-22, 2003.

[13] Nabours, S., Shkolnik, N., Nelms, R., Gnanam, G. et al., "High Efficiency Hybrid Cycle Engine," SAE Technical Paper 2010-01-1110, 2010, doi:10.4271/2010-01-1110.

[14] Shkolnik, N. and Shkolnik, A., "Rotary High Efficiency Hybrid Cycle Engine," SAE Technical Paper 2008-01-2448, 2008, doi:10.4271/2008-01-2448.

[15] Shkolnik, N. and Shkolnik, A., “High Efficiency Hybrid Cycle Engine”, proceedings of the ASME Fall Conference on Internal Combustion Engines, ICEF2005-1221, 2005, doi:10.1115/ICEF2005-1221.

[16] Shkolnik, A., Shkolnik, N., Nabours, S., Nickerson, M., Cho, K., Shah, H., Sapre, C., Louthan, L., Danner, B., and Phillips, E., “Development of the High Efficiency X1 Rotary Diesel Engine”, 2012 Directions in Engine-Efficiency and Emissions Research (DEER) Conference, Michigan, 2012.

[17] de Queiroz Hindi, G. and Pimenta, A., "Numerical Simulation on Influence of the Spray Injector Type in a DISI Engine at Part-Load under Stratified Operation," SAE Technical Paper 2011-36-0026, 2011, doi:10.4271/2011-36-0026.

[18] Šavli, M., “Turbulence kinetic energy - TKE”, University of Ljubljana Faculty of Mathematics and Physics, 2012.

[19] Lin, L., Shulin, D., Jin, X., Jinxiang, W. et al., "Effects of Combustion Chamber Geometry on In-Cylinder Air Motion and Performance in DI Diesel Engine," SAE Technical Paper 2000-01-0510, 2000, doi:10.4271/2000-01-0510.

[20] Sushma, H., Jagadeesha, B.B., “CFD modeling of the in-cylinder flow in Direct-injection Diesel engine”, International Journal of Scientific and Research Publications, Volume 3, Issue 12, December 2013, ISSN 2250-3153.

[21] Martins, F.P., R., C. & Penteado, V., “Simulation and analysis of direct injection strategies for hydrous ethanol in internal combustion engines”, International Journal of Engineering and Innovative Technology, 3(7), 207-215 (2014).

[22] Wang, F., Reitz, R. D., Pera, C., Wang, Z. & Wang, J., “Application of generalized RNG turbulence model to flow in motoring single-cylinder PFI engine”, Engineering Applications of Computational Fluid Mechanics, 7(4), 496-495, (2013).

GLOSSARY

ATV	all-terrain vehicle
BDC	Bottom Dead Center
BMEP	Brake Mean Effective Pressure
CI	Compression Ignition
CR	Compression Ratio
EGR	Exhaust Gas Recirculation
EPO	Exhaust Port Close
FMEP	Friction Mean Effective Pressure
HEHC	High Efficiency Hybrid Cycle
ICE	Internal Combustion Engine
IPC	Intake Port Close
IMEP	Indicated Mean Effective Pressure
MAF	Mass Air Flow
SI	Spark Ignition
TDC	Top Dead Center
TKE	Turbulent Kinetic Energy
UAV	Unmanned Aerial Vehicle

CONTACT INFORMATION

The authors may be reached at info@liquidpiston.com.

ACKNOWLEDGMENTS

The authors wish to thank Northwater Capital Management and Adams Capital Management for funding this development, as well as other members of the engineering / technical team which helped in the design and testing of the X engines, including especially: Adarsh Ganesan, Alexei Sondergeld, Davis Parker, Ritwik Athalye, Tiago João Silva Sousa de Azevedo Costa, Jeremy Serini, Ryan Leary, the team at Century Tool especially Lee Sroczenski. We also would like to thank DARPA for their funding and support.

This research was, in part, funded by the Defense Advanced Research Projects Agency (DARPA). The views, opinions, and/or findings contained in this article/presentation are those of the author(s)/presentor(s) and should not be interpreted as representing the official views or policies of the Department of Defense or the U.S. Government.